SUPPLEMENTAL INFORMATION

Water-Stable Metal-Organic Framework for Hyperpolarized Xenon MRI in Aqueous Solution

Qingbin Zeng[†‡], Zhen Wang[†‡], Qianni Guo[†‡]*, Wei Song[†‡], Xiuchao Zhao[†‡], Yuqi Yang[†‡], Xin Zhou[†‡]*

[†] State Key Laboratory of Magnetic Resonance Spectroscopy and Imaging, National Center for Magnetic Resonance in Wuhan, Wuhan Institute of Physics and Mathematics, Innovation Academy for Precision Measurement Science and Technology, Chinese Academy of Sciences, Wuhan 430071, P. R. China.
[‡] University of Chinese Academy of Sciences, Beijing 100049, P. R. China.

Section 1 Experimental Section

Synthesis procedures

The materials to be added at the start of the reaction are as follows:

60 nm: NH_2-BDC (71.6 mg) and $AlCl_3 \cdot 6H_2O$ (286.1 mg) were dissolved in 7.9 mL MeOH using ultrasound.

120 nm: NH_2-BDC (100.2 mg) and $AlCl_3 \cdot 6H_2O$ (400.5 mg) were dissolved in 7.9 mL MeOH using ultrasound.

250 nm: NH_2-BDC (143.2 mg) and $AlCl_3 \cdot 6H_2O$ (572.2 mg) were dissolved in 7.9 mL MeOH using ultrasound.

320 nm: NH_2-BDC (171.8 mg) and $AlCl_3 \cdot 6H_2O$ (686.6 mg) were dissolved in 7.9 mL MeOH using ultrasound.

510 nm: NH_2-BDC (214.8 mg) and $AlCl_3 \cdot 6H_2O$ (858.3 mg) were dissolved in 7.9 mL MeOH using ultrasound.

Thermal gravimetric analysis (TGA)

All measurements were performed on a TGA analyzer with samples held in aluminum oxide pans in a continuous airflow atmosphere (Balance gas: N_2: 40.0 mL/min, Sample gas: Air: 60.0 mL/min). The samples were heated at a constant rate of 10°C during all TGA experiments.

N_2 adsorption analysis

All N_2 adsorption experiments were performed on a Micromeritics 3 Flex automatic volumetric instrument. A liquid nitrogen bath (77 K) was used for isotherm measurements. Ultra-high purity grade N_2 was used for the adsorption experiments. Before the isotherm measurement, a series of CAU-1 samples were degassed on 3 Flex for 10 h at 120°C. The Brunauer-Emmett-Teller (BET) analysis was performed by plotting $x/v(1-x)$ vs x, where $x = P/P_0$ (P_0 = 1 bar) and v was the volume of nitrogen adsorbed per gram of MOF at standard temperature and pressure (STP). This analysis produced a curve typically consisting of three regions: concave to the x-axis at low pressures, linear at intermediate pressures, and convex to the x-axis at high pressures. The slope

([*c*-1]/v_{mc}) and y-intercept (1/v_{mc}) of this linear region gave the monolayer capacity, v_m, that was then used to calculate the surface area from A = $v_m\sigma_0 N_{AV}$, where σ_0 was the cross-section. All areas of the adsorbate at liquid density (16.2 Å^2 for nitrogen), and N_{AV} was Avogadro's number. Pore size distributions for MOFs were analyzed using quenched non-local density functional theory (NLDFT) based on a carbon model containing slit pores.

Powder X-ray diffraction crystallography

The Powder X-ray Diffraction (PXRD) data of series CAU-1 were collected on a Bruker D8 3 kW diffractometer with Cu-Kα1 X-ray radiation (λ = 1.5406 Å) in transmission geometry.

Hyperpolarized ^{129}Xe NMR

The gas mixture was polarized using a custom-built hyperpolarizer and then bubbled directly into a 10 mm NMR tube containing the MOF sample for 15 s, followed by a 3 s delay to allow the bubbles to collapse. The ^{129}Xe spectra were acquired using a zg pulse sequence (rectangular pulse, pulse length p1 = 31.8 ms).

Section 2 Characterization

TEM of CAU-1

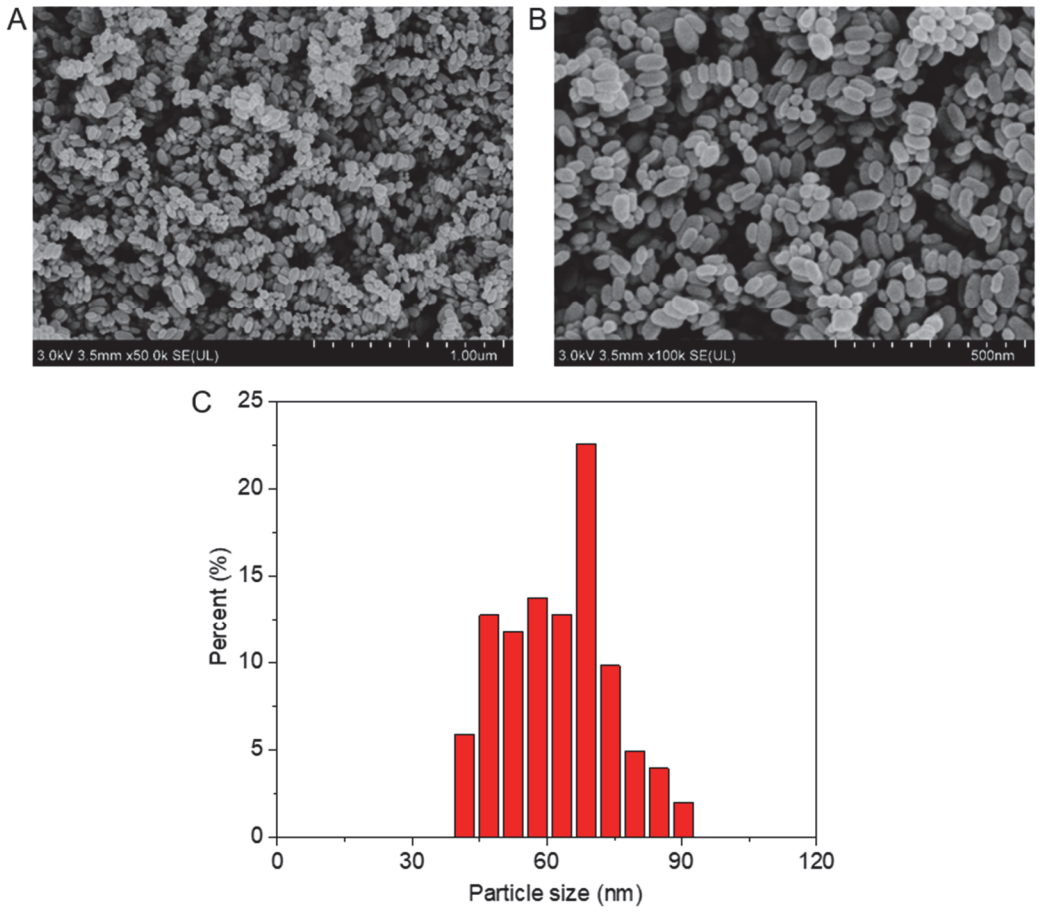

Figure S1. (A) and (B) SEM images of CAU-1 nanoparticles at different scales, scare bars 1 μm and 500 nm, and (C) particle size distribution calculated from SEM images. The average particle size is approximately 60 nm.

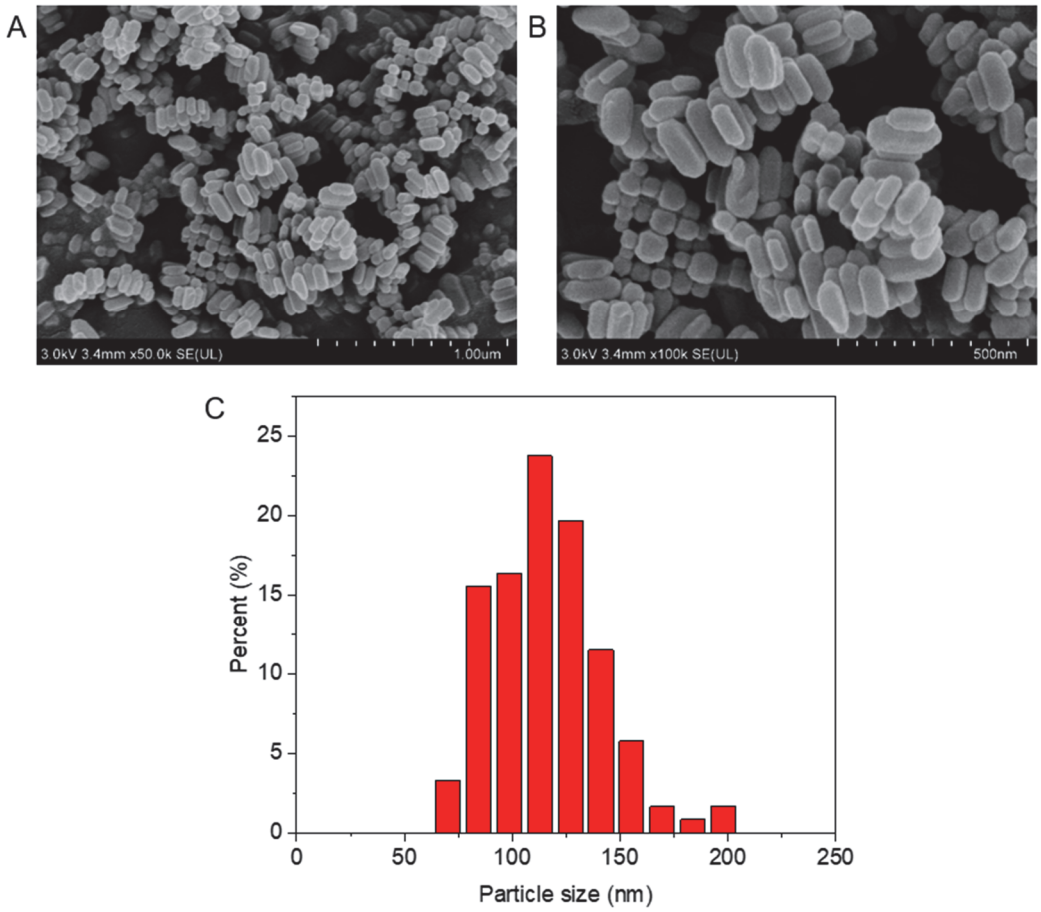

Figure S2. (A) and (B) SEM images of CAU-1 nanoparticles at different scales, scare bars 1 μm and 500 nm, and (C) particle size distribution calculated from SEM images. The average particle size is approximately 120 nm.

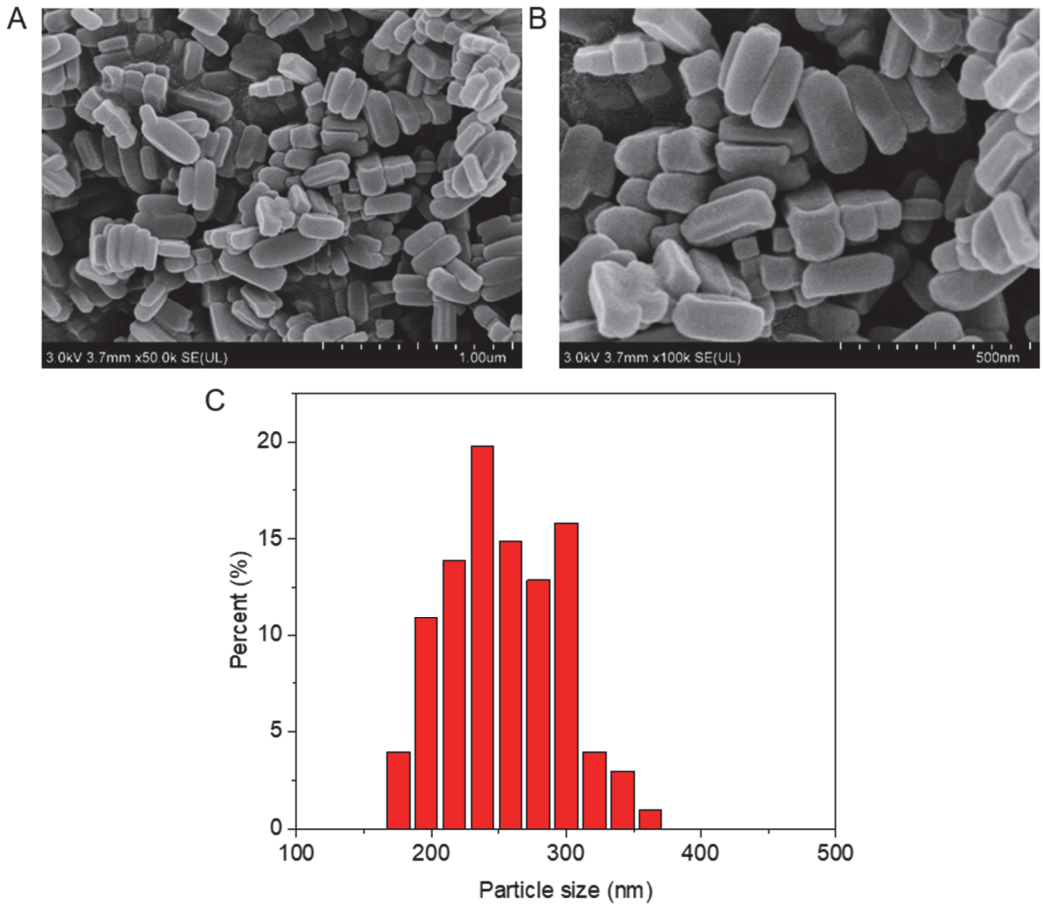

Figure S3. (A) and (B) SEM images of CAU-1 nanoparticles at different scales, scare bars 1 μm and 500 nm, and (C) particle size distribution calculated from SEM images. The average particle size is approximately 250 nm.

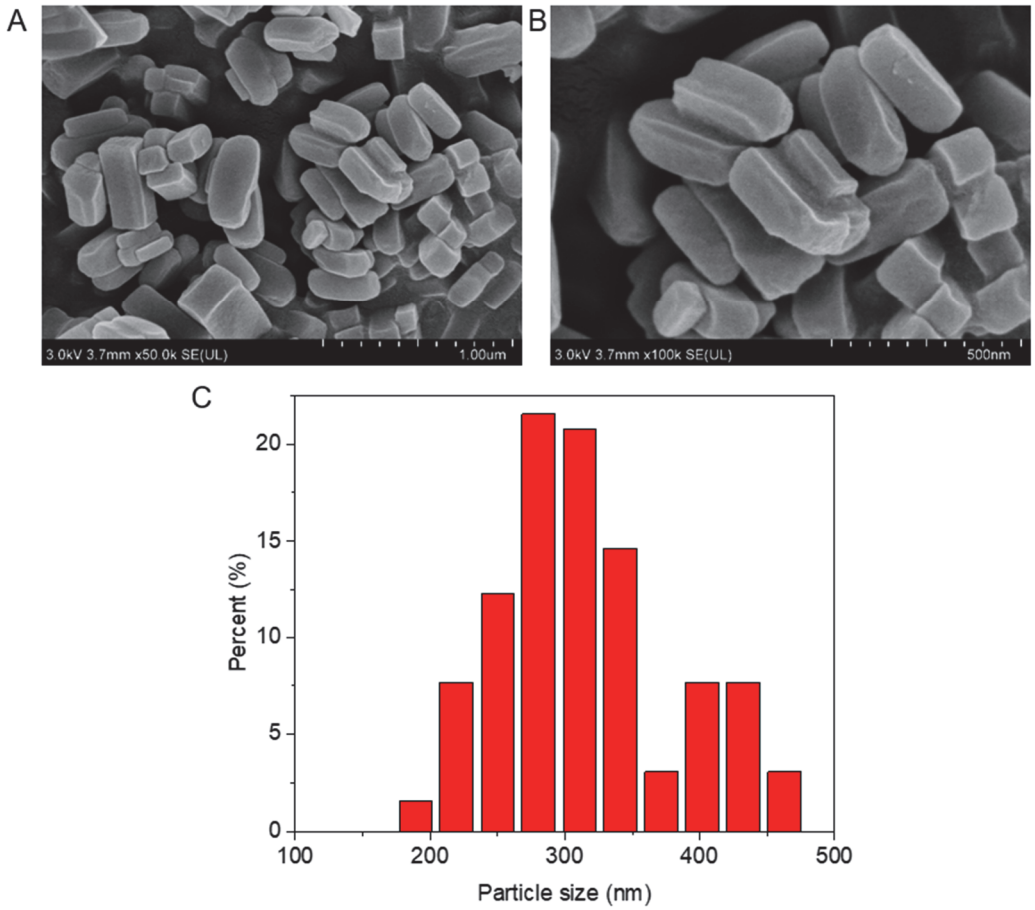

Figure S4. (A) and (B) SEM images of CAU-1 nanoparticles at different scales, scare bars 1 μm and 500 nm, and (C) particle size distribution calculated from SEM images. The average particle size is approximately 320 nm.

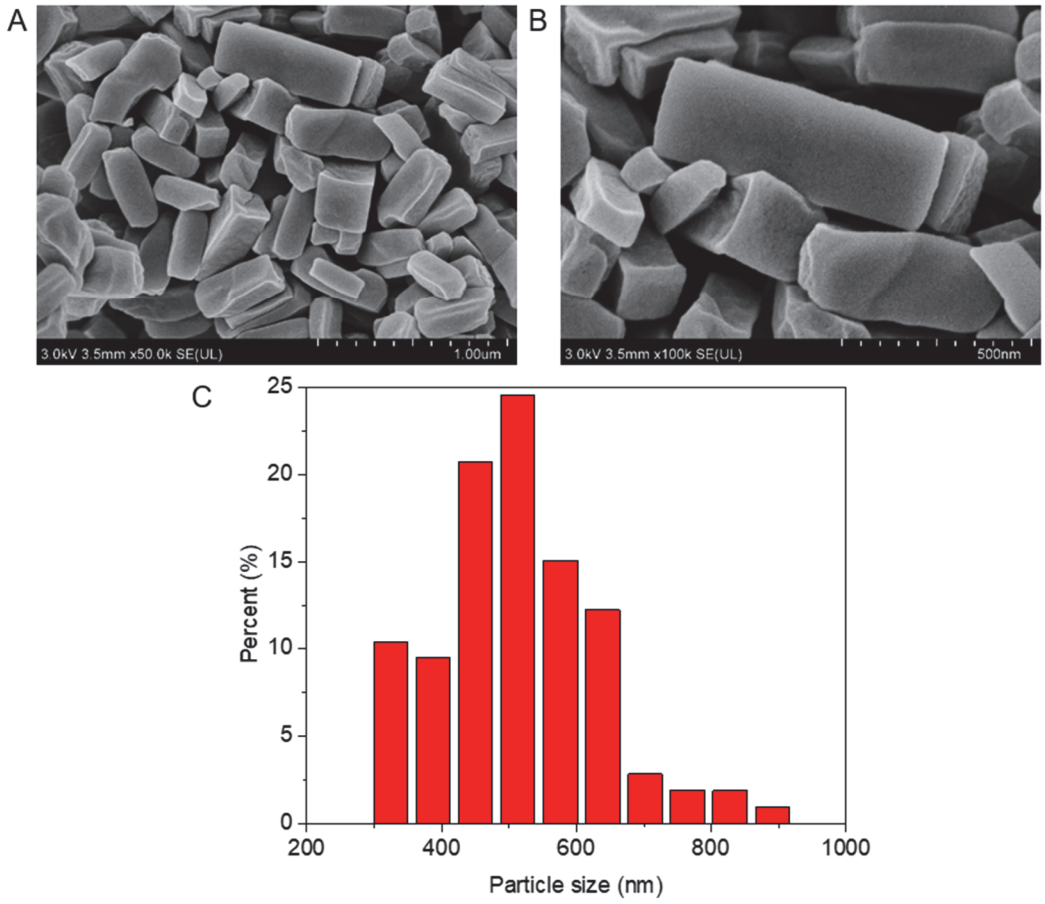

Figure S5. (A) and (B) SEM images of CAU-1 nanoparticles at different scales, scare bars 1 μm and 500 nm, and (C) particle size distribution calculated from SEM images. The average particle size is approximately 510 nm.

PXRD of CAU-1

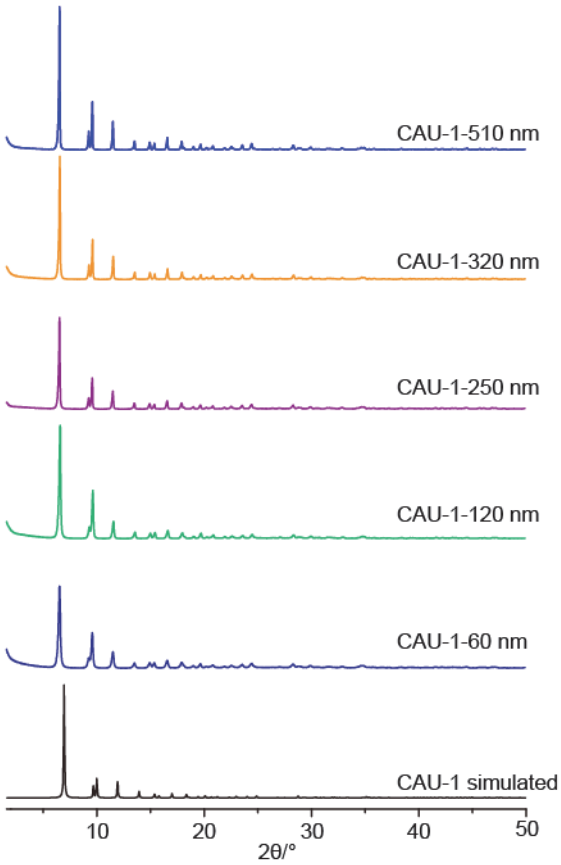

Figure S6. Comparisons of the experimental PXRD pattern of activated CAU-1 in different particle sizes (60, 120, 250, 320, and 510 nm) with the simulated diffraction pattern (black) (Cu Kα λ = 1.5406 Å).

FT-IR spectroscopy of CAU-1

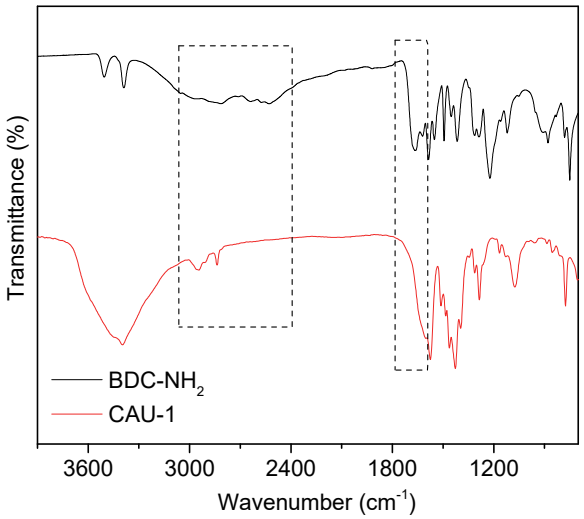

Figure S7. Fourier-transform infrared (FT-IR) spectroscopy of CAU-1 and 2-aminoterephthalic acid.

N_2 adsorption isotherms of CAU-1

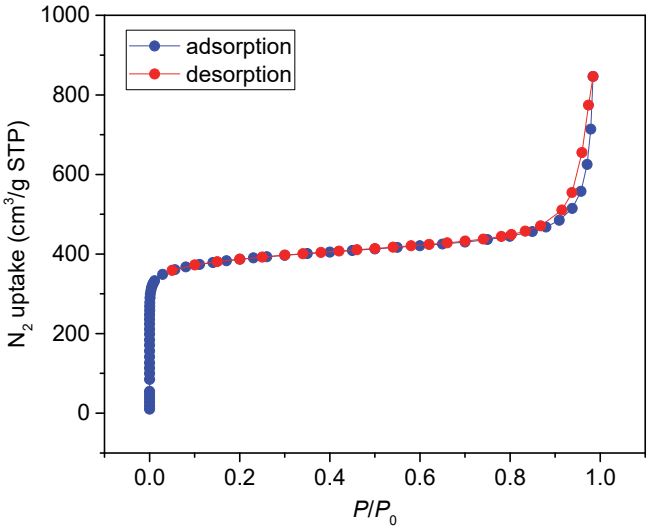

Figure S8. Nitrogen isotherm of CAU-1 (particle size 60 nm) at 77 K. Blue and red symbols represent absorption and desorption branches, respectively. Points are connected to provide a clear shape of the isotherm.

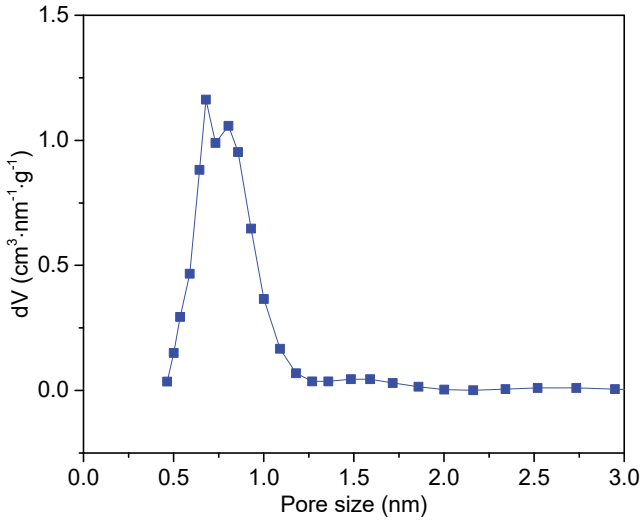

Figure S9. Pore size distribution analysis of CAU-1 (particle size 60 nm) based on the corresponding N_2 isotherms.

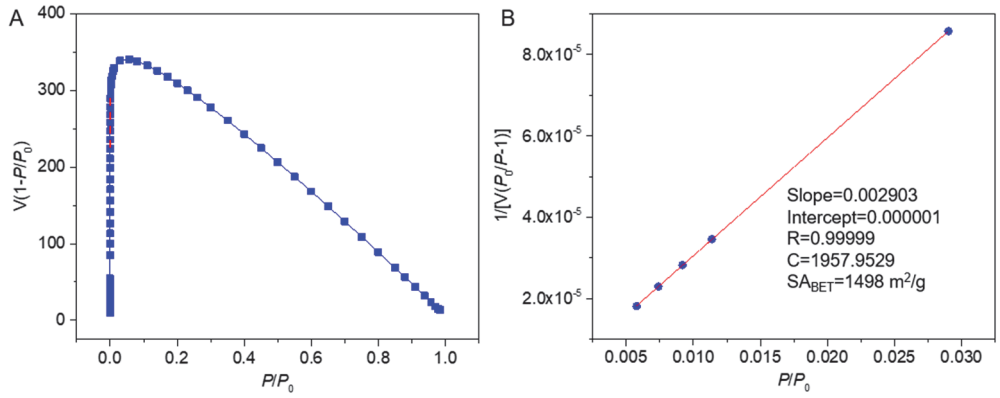

Figure S10. BET area calculation for CAU-1 (particle size 60 nm) based on nitrogen isotherm at 77 K. (A) The points between the dashed lines are selected based on the first consistency criterion, (B) Plot showed good fitting of the BET model.

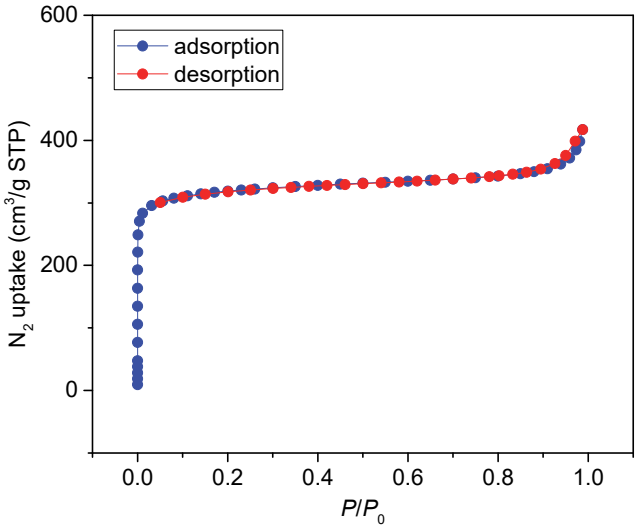

Figure S11. Nitrogen isotherm of CAU-1 (particle size 120 nm) at 77 K. Blue and red symbols represent absorption and desorption branches, respectively. Points are connected to provide a clear shape of the isotherm.

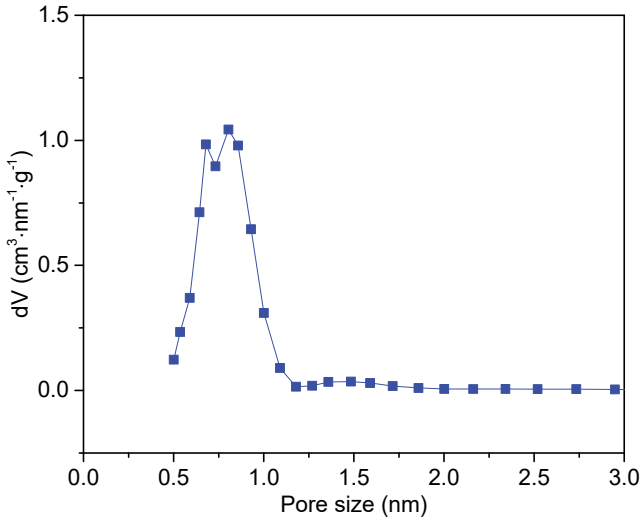

Figure S12. Pore size distribution analysis of CAU-1 (particle size 120 nm) based on the corresponding N_2 isotherms.

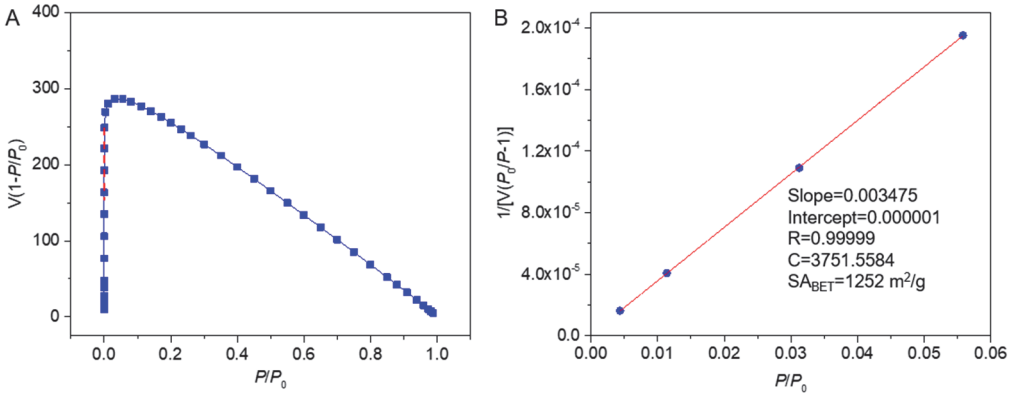

Figure S13. BET area calculation for CAU-1 (particle size 120 nm) based on nitrogen isotherm at 77 K. (A) The points between the dashed lines are selected based on the first consistency criterion, (B) Plot showed good fitting of the BET model.

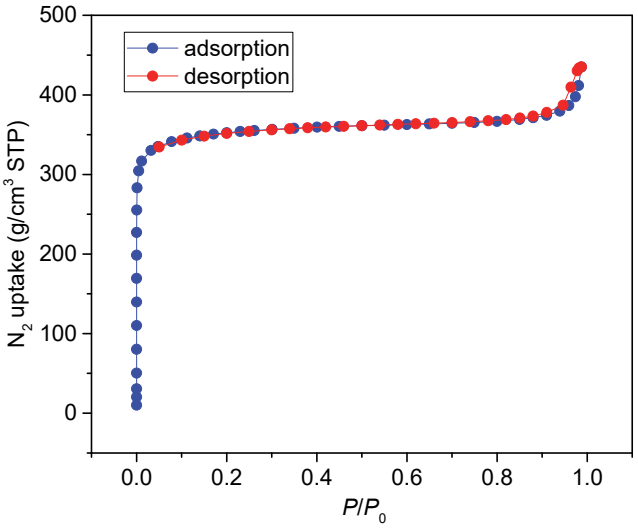

Figure S14. Nitrogen isotherm of CAU-1 (particle size 250 nm) at 77 K. Blue and red symbols represent absorption and desorption branches, respectively. Points are connected to provide a clear shape of the isotherm.

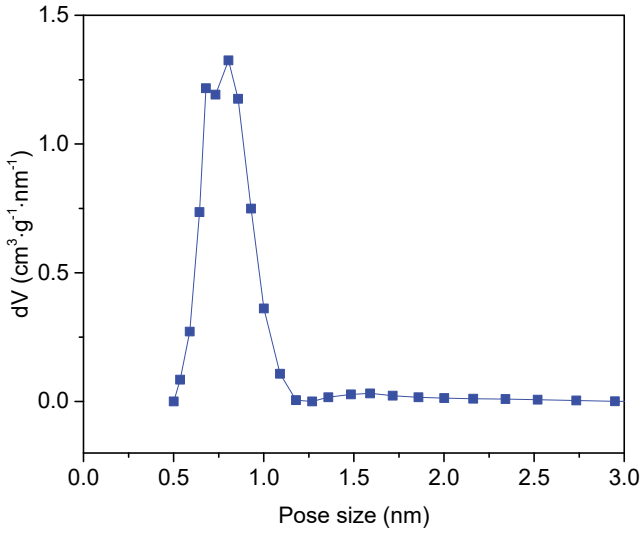

Figure S15. Pore size distribution analysis of CAU-1 (particle size 250 nm) based on the corresponding N_2 isotherms.

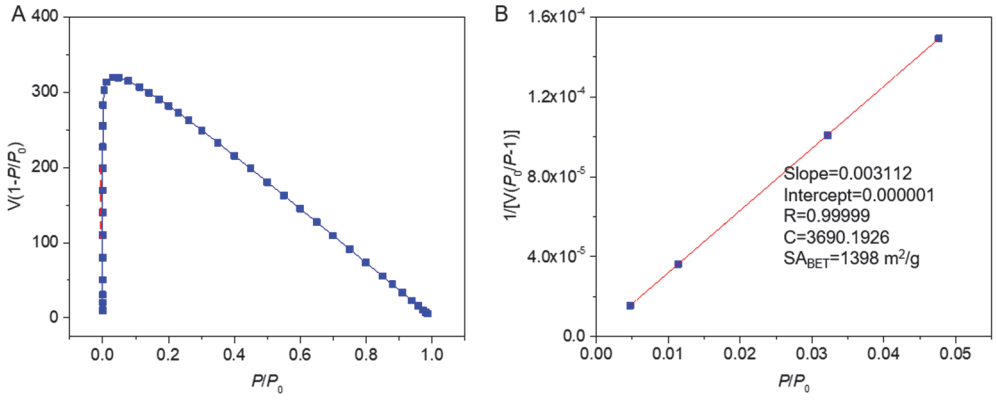

Figure S16. BET area calculation for CAU-1 (particle size 250 nm) based on nitrogen isotherm at 77 K. (A) The points between the dashed lines are selected based on the first consistency criterion, (B) Plot showed good fitting of the BET model.

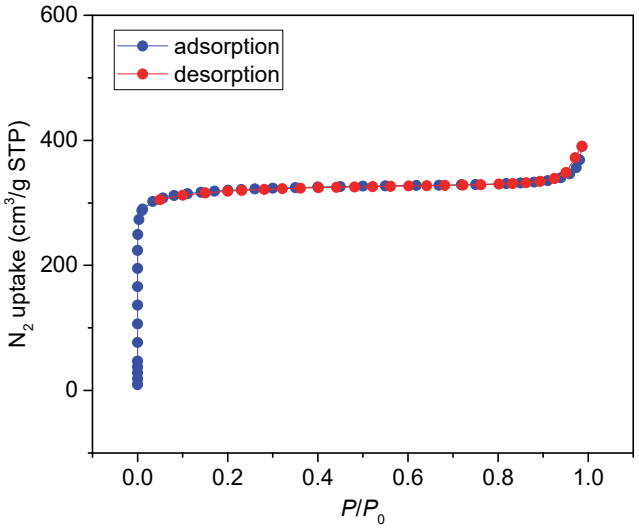

Figure S17. Nitrogen isotherm of CAU-1 (particle size 320 nm) at 77 K. Blue and red symbols represent absorption and desorption branches, respectively. Points are connected to provide a clear shape of the isotherm.

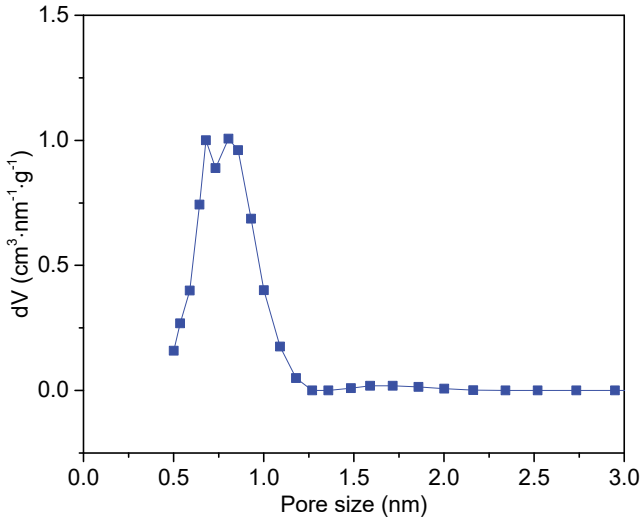

Figure S18. Pore size distribution analysis of CAU-1 (particle size 320 nm) based on the corresponding N_2 isotherms.

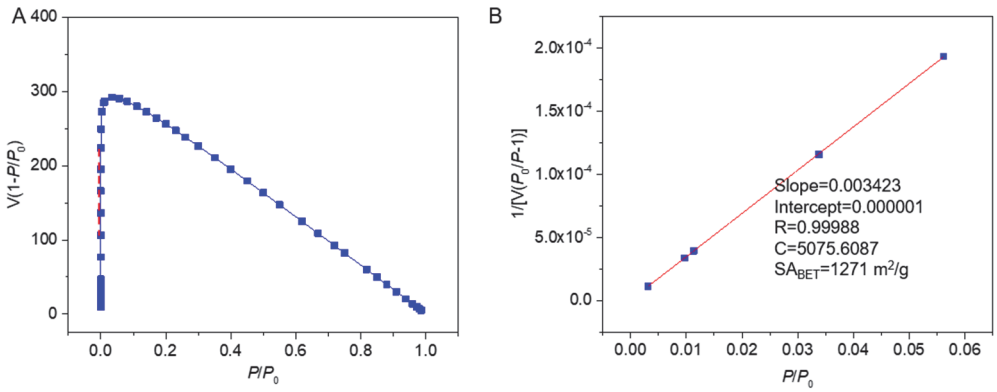

Figure S19. BET area calculation for CAU-1 (particle size 320 nm) based on nitrogen isotherm at 77 K. (A) The points between the dashed lines are selected based on the first consistency criterion, (B) Plot showed good fitting of the BET model.

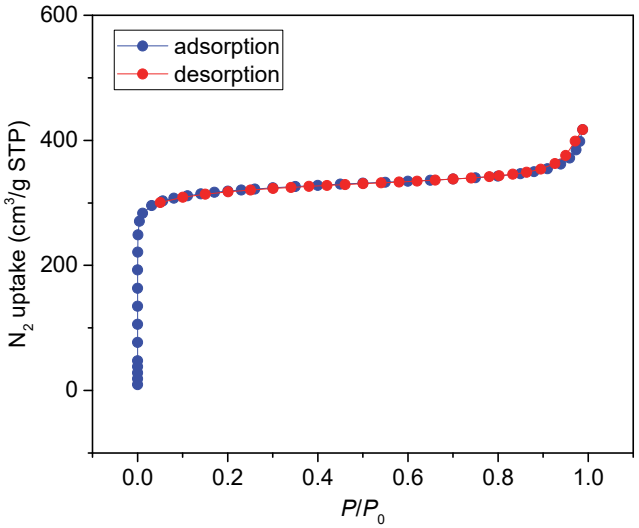

Figure S20. Nitrogen isotherm of CAU-1 (particle size 510 nm) at 77 K. Blue and red symbols represent absorption and desorption branches, respectively. Points are connected to provide a clear shape of the isotherm.

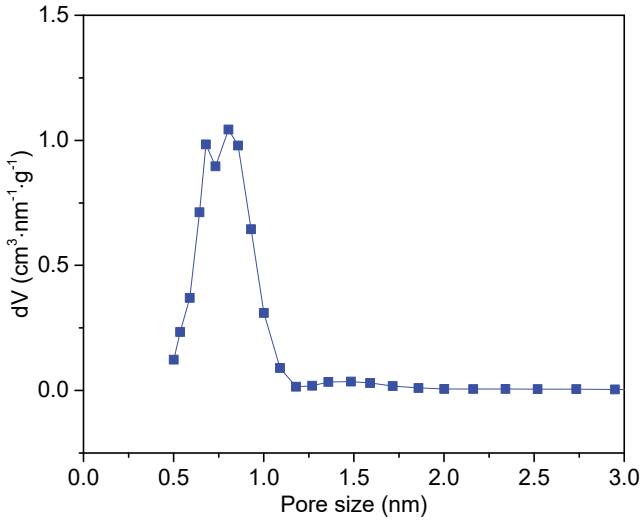

Figure S21. Pore size distribution analysis of CAU-1 (particle size 510 nm) based on the corresponding N_2 isotherms.

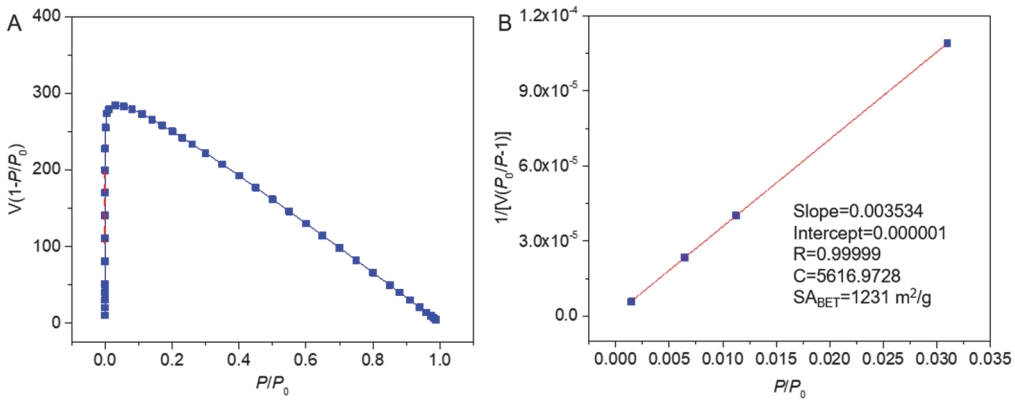

Figure S22. BET area calculation for CAU-1 (particle size 510 nm) based on nitrogen isotherm at 77 K. (A) The points between the dashed lines are selected based on the first consistency criterion, (B) Plot showed good fitting of the BET model.

Thermo gravimetric analysis (TGA) of CAU-1

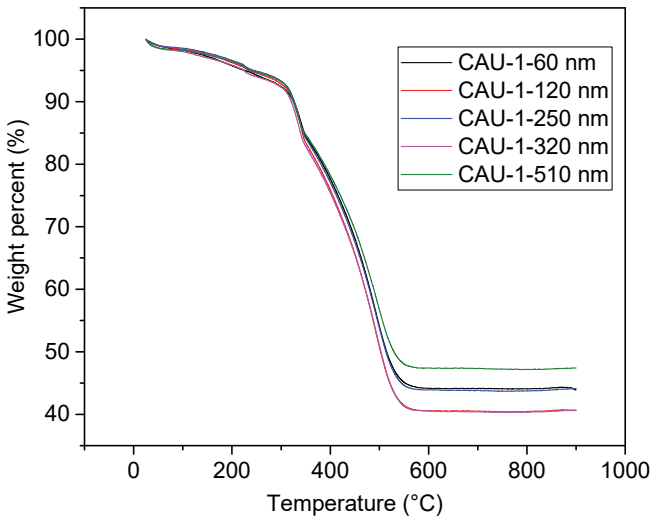

Figure S23. TGA trace of activated series of MOFs. In each TGA plot, the small weight loss before 100°C was attributed to the evaporation of water introduced into MOF from air during the sample mounting. The major weight loss evidenced (around 300°C) was caused by the destruction of CAU-1 series. The thermal stability of these MOF samples was demonstrated by thermo gravimetric analysis (TGA) in air where no obvious structure decomposition was observed until 300°C.

Section 3 Experiments

Hyperpolarized ^{129}Xe MRI for CAU-1

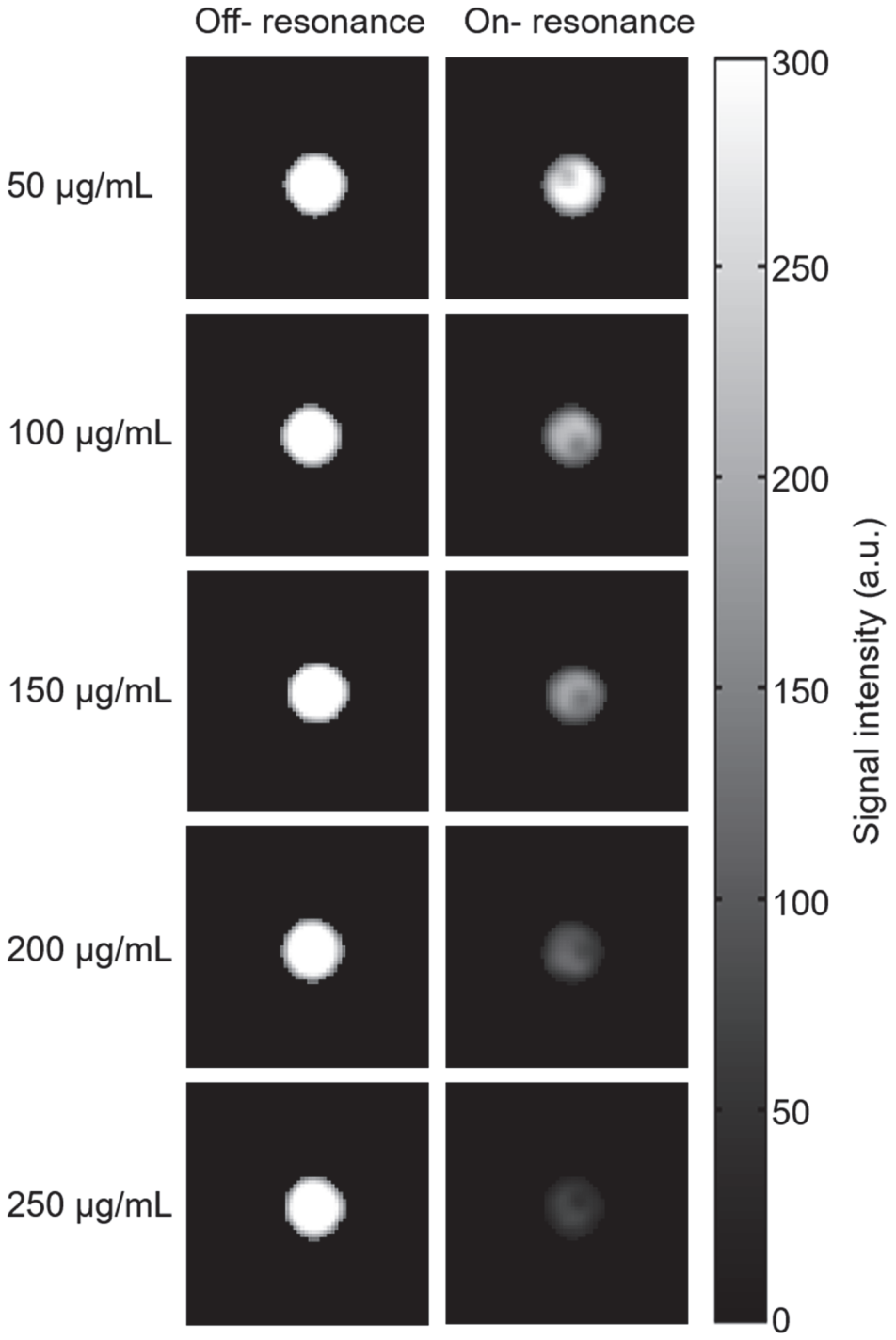

Figure S24. Hyperpolarized ^{129}Xe MRI for different concentrations of CAU-1.

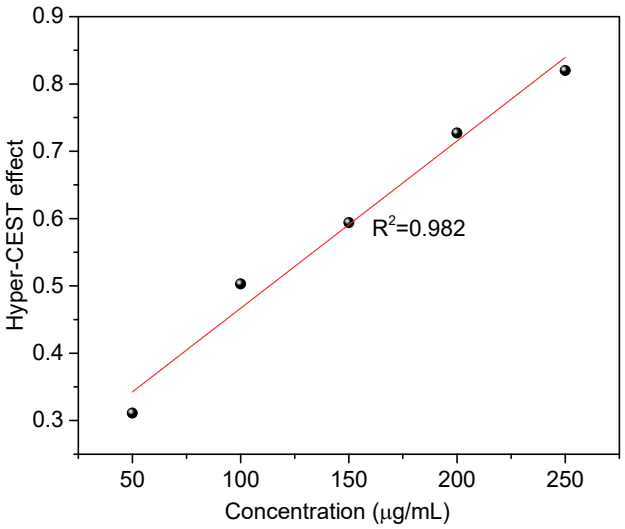

Figure S25. The average Hyper-CEST effect of different concentrations of CAU-1 in aqueous solution. The Hyper-CEST effect was calculated based on the average of 4 on-resonant (saturation on Xe @ cage: -41 ppm) and 4 off-resonant (saturation at 41 ppm) images (The chemical shift of dissolved ^{129}Xe was set as 0 ppm).

Water-stability for CAU-1

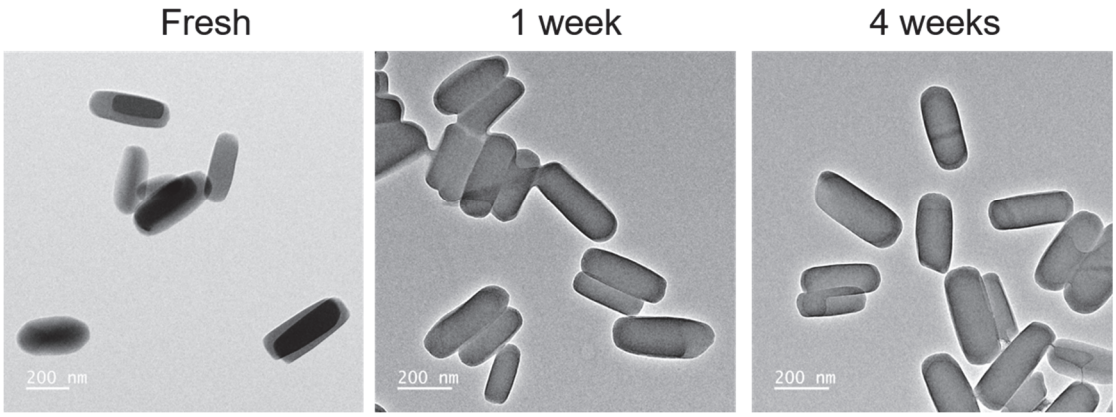

Figure S26. TEM for CAU-1 after immersion in water for different days.

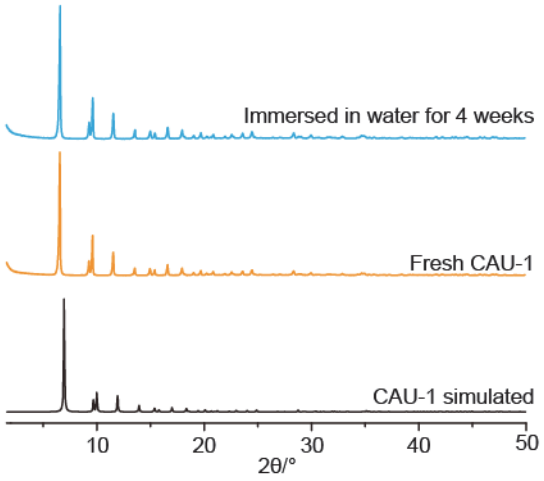

Figure S27. PXRD for CAU-1 after immersion in water for different days.

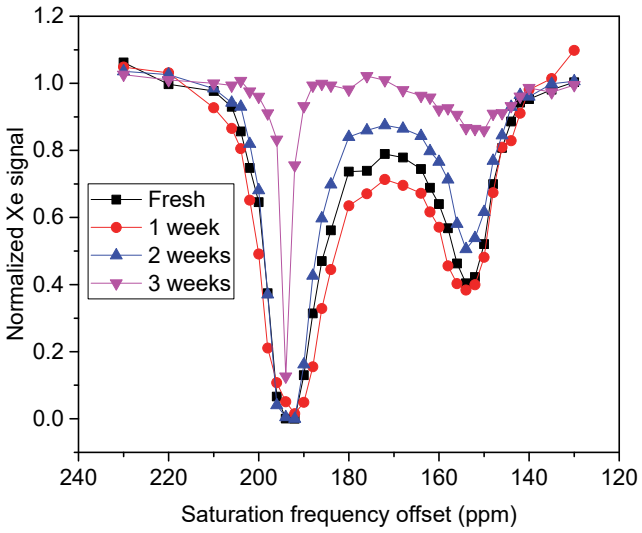

Figure S28. Hyper-CEST spectra for CAU-1 after immersion in water for different days.

Hyper-CEST for CAU-1 at different saturation power

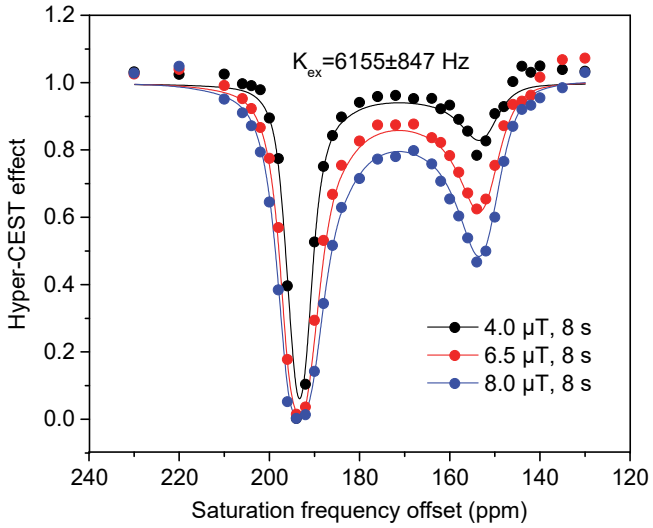

Figure S29. Quantitatively analyzes the chemical exchange saturation transfer of ^{129}Xe in CAU-1. The exchange rate of the entrapped Xe to the dissolved Xe is 6155±847Hz.

Zeta potential for CAU-1 at different pH values

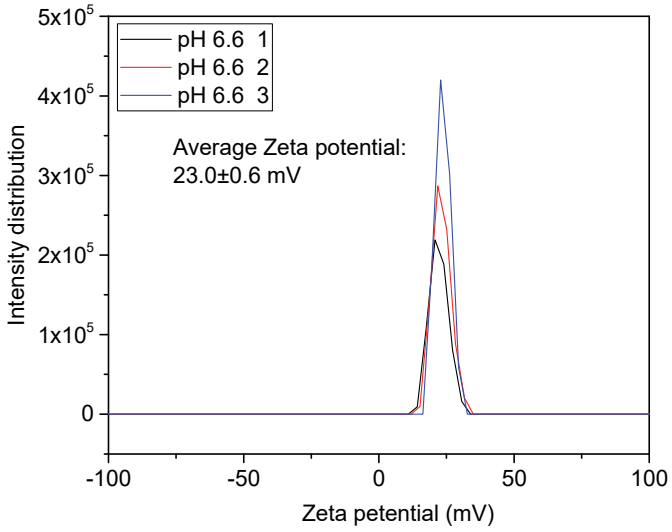

Figure S30. Zeta potential of CAU-1 in aqueous solution at pH 6.6, the test was repeated three times.

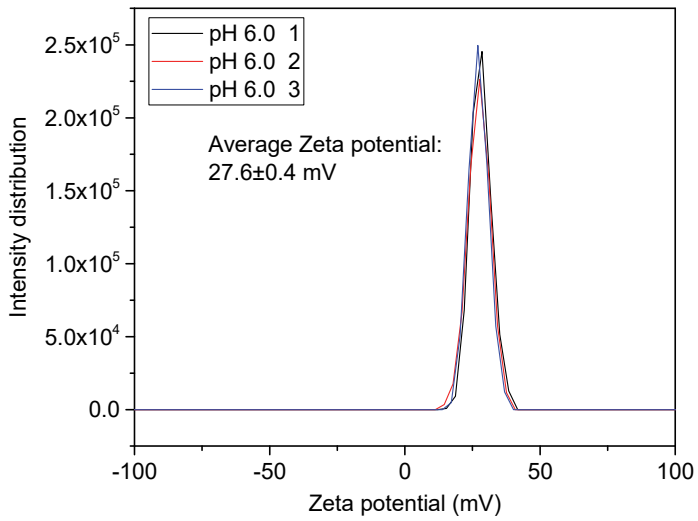

Figure S31. Zeta potential of CAU-1 in aqueous solution at pH 6.0, the test was repeated three times.

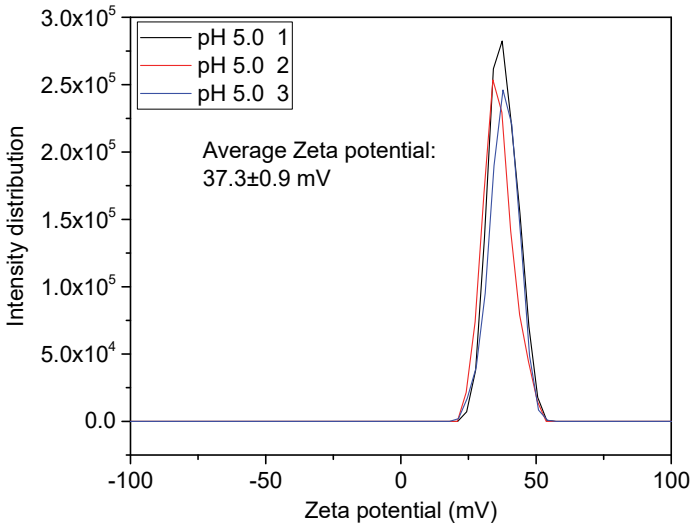

Figure S32. Zeta potential of CAU-1 in aqueous solution at pH 5.0, the test was repeated three times.

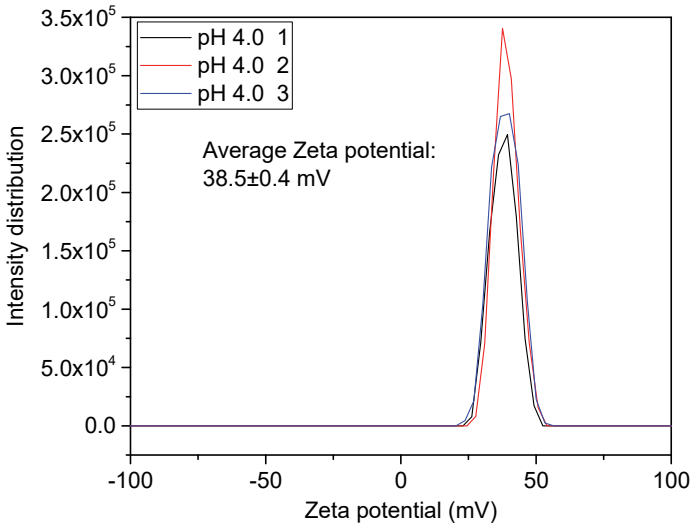

Figure S33. Zeta potential of CAU-1 in aqueous solution at pH 4.0, the test was repeated three times.

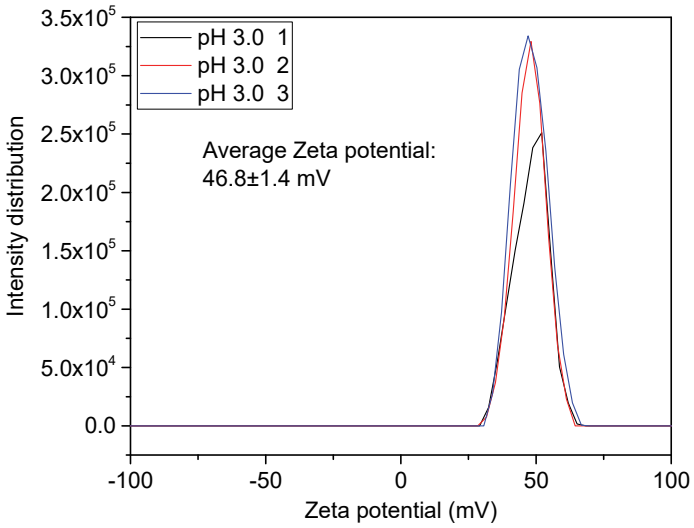

Figure S34. Zeta potential of CAU-1 in aqueous solution at pH 3.0, the test was repeated three times.

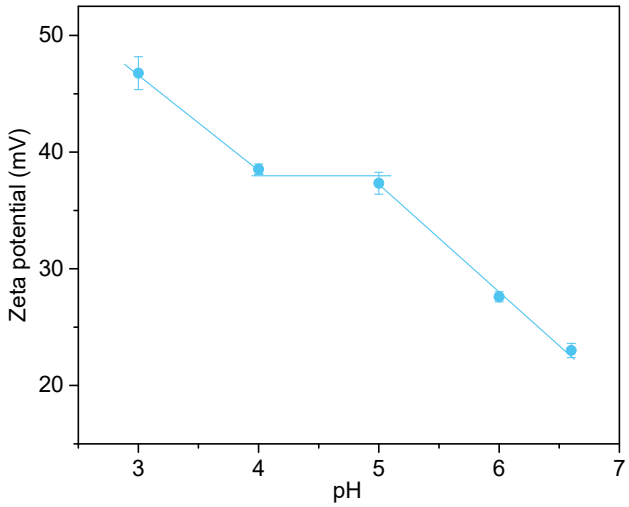

Figure S35. The pH-dependent Zeta potential of CAU-1 in aqueous solution. SD is based on three different tests.

DLS particle size for CAU-1 at different pH values

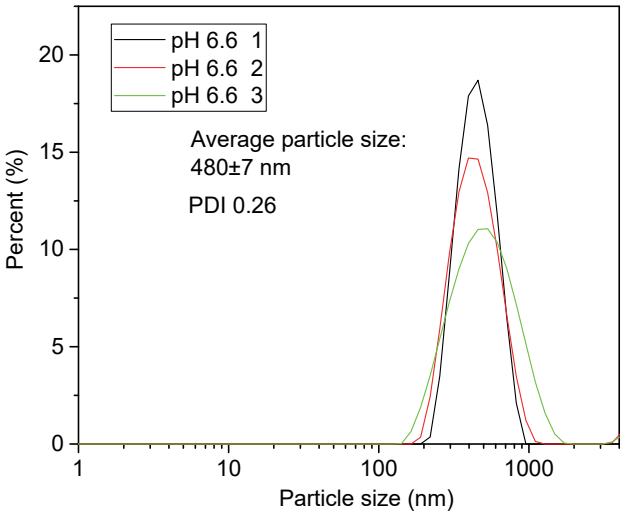

Figure S36. DLS size distribution of CAU-1 nanoparticles in water at pH 6.6, the test was repeated three times.

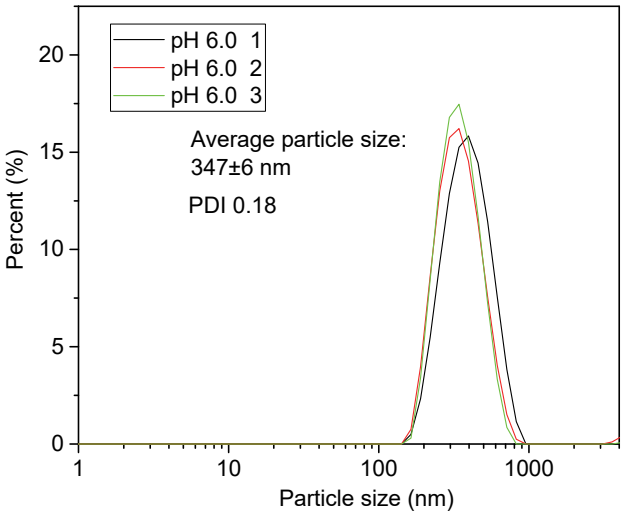

Figure S37. DLS size distribution of CAU-1 nanoparticles in water at pH 6.0, the test was repeated three times.

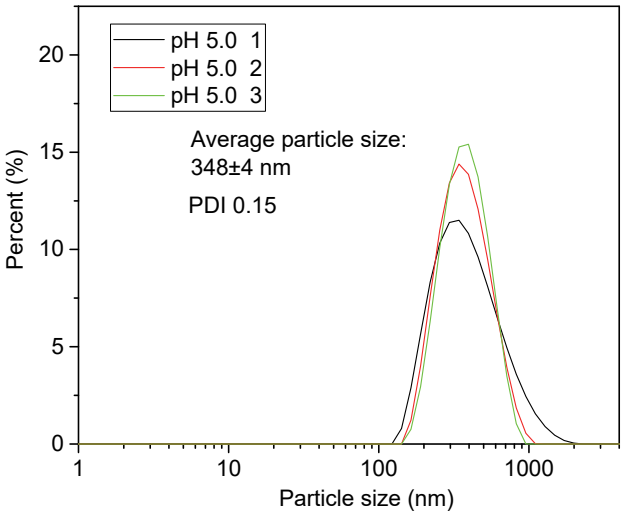

Figure S38. DLS size distribution of CAU-1 nanoparticles in water at pH 5.0, the test was repeated three times.

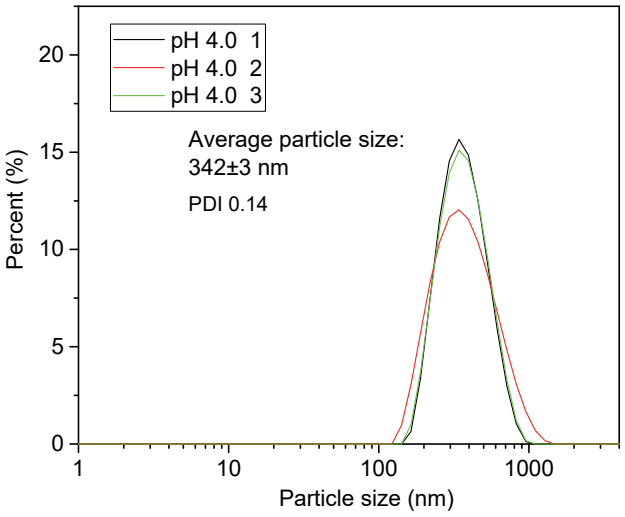

Figure S39. DLS size distribution of CAU-1 nanoparticles in water at pH 4.0, the test was repeated three times.

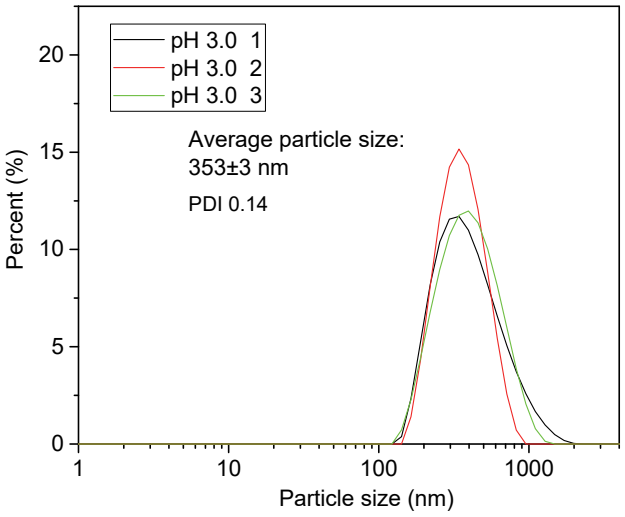

Figure S40. DLS size distribution of CAU-1 nanoparticles in water at pH 3.0, the test was repeated three times.

Table S1. The summary of the pore sizes, pore volumes, and BET surface area in different MOF samples.

Sample	Pore size (Å)		Total pore volume (cm^3/g)	BET surface area (m^2/g)
CAU-1-60 nm	0.679	0.804	1.309	1498
CAU-1-120 nm	0.679	0.804	0.645	1252
CAU-1-250 nm	0.679	0.804	0.673	1398
CAU-1-320 nm	0.679	0.804	0.604	1271
CAU-1-510 nm	0.679	0.804	0.577	1231